An Articulating Statistical Shape Model of the Human Hand

Van Houtte, Jeroen; Stanković, Kristina ; Booth, Brian G.; Danckaers, Femke ; Bertrand, Véronique; Verstreken, Frederik; Sijbers, Jan; Huysmans, Toon

DOI
10.1007/978-3-319-94223-0_41

Publication date
2019

Document Version
Final published version

Published in
Advances in Human Factors in Simulation and Modeling

Citation (APA)
Van Houtte, J., Stanković, K., Booth, B. G., Danckaers, F., Bertrand, V., Verstreken, F., Sijbers, J., & Huysmans, T. (2019). An Articulating Statistical Shape Model of the Human Hand. In D. N. Cassenti (Ed.), *Advances in Human Factors in Simulation and Modeling: Proceedings of the AHFE 2018 International Conferences on Human Factors and Simulation and Digital Human Modeling and Applied Optimization* (pp. 433-445). (Advances in Intelligent Systems and Computing ; Vol. 780). Springer. https://doi.org/10.1007/978-3-319-94223-0_41

An Articulating Statistical Shape Model of the Human Hand

Jeroen Van Houtte[1(✉)], Kristina Stanković[1], Brian G. Booth[1], Femke Danckaers[1], Véronique Bertrand[2], Frederik Verstreken[2], Jan Sijbers[1], and Toon Huysmans[1,3]

[1] imec-Vision Lab, University of Antwerp, 2610 Antwerp, Belgium
Jeroen.vanhoutte@uantwerp.be
[2] Orthopedic Department, AZ Monica Hospital, 2000 Antwerp, Belgium
[3] Applied Ergonomics and Design, Delft University of Technology, 2628 Delft, The Netherlands

Abstract. This paper presents a registration framework for the construction of a statistical shape model of the human hand in a standard pose. It brings a skeletonized reference model of an individual human hand into correspondence with optical 3D surface scans of hands by sequentially applying articulation-based registration and elastic surface registration. Registered surfaces are then fed into a statistical shape modelling algorithm based on principal component analysis. The model-building technique has been evaluated on a dataset of optical scans from 100 healthy individuals, acquired with a 3dMD scanning system. It is shown that our registration framework provides accurate geometric and anatomical alignment, and that the shape basis of the resulting statistical model provides a compact representation of the specific population. The model also provides insight into the anatomical variation of the lower arm and hand, which is useful information for the design of well-fitting products.

Keywords: Articulation-model · Registration · Human hand
Statistical shape modelling

1 Introduction

Shape models of faces and full-bodies have become valuable for many commercial applications of computer vision and graphics, ranging from customized design to motion tracking [1, 2]. Their potential for noise and artifact reduction, hole filling, and resolution improvement, have aided to employ low-budget scanners with low mesh quality [3, 4]. Recently, the popularity of these techniques has led to their consideration for modelling the human hand, most often for the task of hand tracking [5, 6].

In the context of hand tracking, shape models have been used with the primary goal of improving pose estimation [5–9]. In general, these techniques consist of a fixed prior rigged template model which can be aligned to person-specific depth images or 3D meshes. The alignment is often achieved by solving for the articulation and anthropometric parameters of the template that optimally match the subject's depth image or

D. N. Cassenti (Ed.): AHFE 2018, AISC 780, pp. 433–445, 2019.
https://doi.org/10.1007/978-3-319-94223-0_41

3D mesh. The registration is regularized by principal component analysis (PCA) [5] or by an "as rigid as possible" (ARAP)-regularization [6].

As the focus of these techniques has been on obtaining accurate pose information, the level of geometric detail can vary significantly between models. Many models are composed of primitives like spheres and cylinders of fixed size, with the registration step simply articulating these primitives [5, 7]. Others use a more realistic skin geometry, but only allow the model to articulate [8]. Accommodating variations in hand shape and size has only recently been explored [6, 9], and those variations have not been restricted to a range of "natural" hand shapes and sizes.

It has been argued that detailed personalized hand models improve the accuracy of both model registration and pose estimation [10]. This argument was furthered by Khamis et al. who regularized possible hand shapes with a low-dimensional parametric shape model that included statistical shape variations of a population [11]. Ideally, this shape model would be based on a dataset of high-quality surface scans in the same pose, but Khamis et al. constructed their shape basis on low-quality depth scans which contained self-occlusions. To address the low quality, their statistical shape model was estimated simultaneously with each individual's hand shape and pose parameters.

Meanwhile, recent advances in optical scanning technology, such as the 3dMD-system [12], have enabled the acquisition of high-quality (<0.5 mm error) 3D surface scans, even from highly articulating objects like hands. It is expected that a statistical shape model based on these high-quality scans would reveal more geometric details and it is therefore the interest of this paper to build a high-resolution geometric shape basis that, to the best of our knowledge, has not been seen in the literature.

Building such as statistical model requires bringing the 3D scans of different subjects' hands into anatomical correspondence. Having an anatomical correspondence for all points of all meshes is critical to build an accurate and interpretable model. However, this is an especially difficult task for a complex articulating shape like the hand.

The aim of this study is to obtain reliable anatomical correspondence for building a statistical human hand model. We propose a registration algorithm, similar to the technique in [9], that aligns a template articulation model to a database containing 100 high-quality 3D scans of human hands. We hypothesize that the addition of the articulation model, and its corresponding registration algorithm, will allow us to more accurately obtain shape correspondences, and normalize for pose, in 3D scans of human hands. We further hypothesize that these advances in shape correspondences and pose normalization will facilitate the use of standard statistical shape modelling algorithms, like PCA, on 3D scans of human hands.

2 Methods

At a high level, our proposed shape modelling technique works as follows. An articulating reference of the human hand, with anatomically correct rotation axes, angles, and constraints, is constructed to act as prior in an articulation-based registration method. This reference hand is then registered to each optical surface scan of a database in order to make anatomically correct correspondences between them. Person-specific

deviations that cannot be captured by the reference are accommodated through a subsequent elastic surface registration step. Finally, the registered surfaces are articulated to the same pose and PCA is used to derive the statistical shape model of the human hand. The following subsections discuss these steps in further detail.

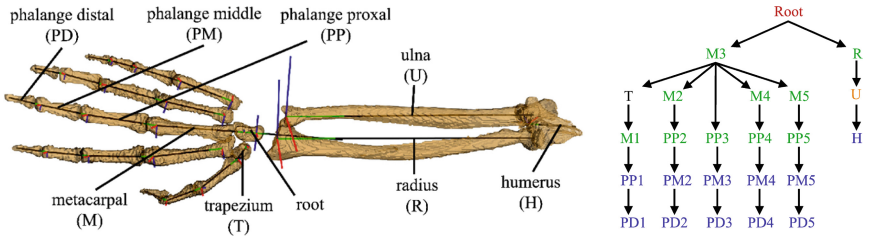

(a) Arm skeleton, with labelled bones (b) Bone hierarchy

Fig. 1. Our reference articulating hand model is defined by the skeleton in (a). The bones in this skeleton are ordered in the hierarchical tree structure in (b) with an artificial root bone at the wrist. Arrows indicate the parent-child relationship. Colors indicate the corresponding articulation parameters: α(blue), α and β(green), γ(red), δ(orange). See text for further details.

2.1 Reference Articulating Hand Model

Reference Surface Geometry and Skeleton. Our reference hand is based on a single Magnetic Resonance Image (MRI) scan of the first author's right hand (repetition time [TR]: 4220 ms; echo time [TE]: 1560 ms; field of view [FOV]: 192 mm $\times$ 520 mm; resolution: 1 mm^3; no gap). The outer skin surface and all relevant bones were manually segmented from the MR image.

To construct the surface mesh of the reference hand, the binary label field of each body part, obtained from the MRI scan, was then converted to a triangulated surface mesh using a discrete marching cube algorithm [13]. The extracted skin surface mesh was then removed of noisy outliers, smoothed in volume-preserving way [14] and remeshed uniformly [15]. The reference skin mesh is denoted by $\widehat{\mathrm{M}}_M = (\widehat{V}_M, \varepsilon_M)$, with $\hat{V}_M \in \mathbb{R}^{3\times \mathrm{N_M}}$ a matrix containing the coordinates of the N_M vertices in a rest pose (the rest pose being denoted by the hat), and $\varepsilon_M \in \mathbb{R}^{N_M \times N_M}$ representing the connectivity, which remains constant at all times.

An abstract line-skeleton $\hat{S}$, defined using the set of segmented bones, is shown in Fig. 1(a). Each segmented bone b is represented by a local coordinate frame in the skeleton (i.e. an origin and orientation). The origin of the bone is located at its center-of-rotation $\boldsymbol{h_b}$ and the orientation of its coordinate frame is as described by the International Society of Biomechanics (ISB) [16]. The orientation of each bone with respect to the world reference frame is described by the world-to-bone rotation matrix $C_b \in SO(3)$.

Bone Hierarchy. The set of bones are ordered in the hierarchical tree structure shown in Fig. 1(b). This hierarchy represents the parent-child relationships between the coordinate frames of each bone in the skeleton. The root of the hierarchy is an artificial bone located at the wrist with the same orientation as the third metacarpal bone. A wrist-rooted armature allows us to describe arm and hand motion independently from each other, but with respect to a common root coordinate system at the wrist (this decoupling will be a benefit in our registration tasks). Global hand motion is described by the third metacarpal bone, which the ISB standard defines as the parent of all other carpal bones [16].

Articulation. The articulation of the hand is defined by the state of its joints. Using our skeleton, the state of each joint can be described as a rotation between the local coordinate frames of adjacent bones:

$$R_b = C_b C_{p(b)}^{-1}, \tag{1}$$

where $p(b)$ is the parent of bone b as defined by the tree structure in Fig. 1(b). The rotation matrix R_b captures how bone b is articulated with respect to its parent. This matrix can be decomposed into three rotation angles - $\alpha_b, \beta_b, \gamma_b$ - which match the ISB's joint angle descriptions [16]. The angle α_b is the primary angle of articulation and describes the bending of the fingers and flexion/extension of the wrist. The angle β is the secondary angle of articulation and describes ulnar/radial deviations of the wrist and the separation between the fingers. The angle γ is a roll angle around the bone's longitudinal axis. An additional angle, δ, is used to define pronation-supination of the arm. This motion is modelled as a rotation around an axis connecting the ulna at the wrist to the radius at the elbow. In the wrist-centered armature the ulna rotates around this axis over the radius. The degrees of freedom for each bone have been indicated by the color in Fig. 1(b): α(blue), α and β(green), γ(red), δ(orange).

When articulating a bone with a new set of angles, we recalculate the parent to bone rotation matrix as a concatenation of these rotation angles. From Eq. (1) it is possible to update the rotation matrix R_b since its parent maintained the same position in space. Relating the rotation matrix of the rest pose with this of the articulated pose, provides the rest-to-pose rotation matrix:

$$T_b = C_b \hat{C}_b^{-1} \tag{2}$$

from which we can update the head position of the bone and update the bones further down in the tree hierarchy.

Finally, we confine, by visual inspection, all joint articulation angles to remain within a natural range of motion. To accomplish this, we introduce a mapping from these constrained physical angles to "dummy" unconstrained variables as described in [17]. The benefit of the "dummy" unconstrained variable is that it can be optimized in the registration algorithm without any changes to the optimizer.

Anthropometric Scaling. Besides the articulation of the skeleton, the reference model also accommodates the anthropometric variations related to bone length and body part

thickness. The model therefore adopts an affine scaling of each bone defined by a longitudinal scaling factor $s^{//}$ and a transversal scaling factor $s^{\perp}$. The scaling matrix in world coordinates can be written as follows:

$$S_b = C_b \, diag\left(s_b^{\perp}, s_b^{//}, s_b^{\perp}\right) C_b^{-1}. \tag{3}$$

The world to bone transformation including both articulation and scaling is therefore defined as:

$$F_b = S_b T_b. \tag{4}$$

In the reference hand, we apply longitudinal and transversal scaling on the lower arm, hand palm, and each finger separately. For the fingers, a single longitudinal scaling factor is used for all phalanges of the same digit; this is justified by the fact that the ratio of bone lengths between phalanges of a single digit obey closely the golden ratio rule [18]. Nevertheless, we allow the metacarpals to change in length independently from the phalanges in order to maintain flexibility of the reference during the registration task.

Skinning. To deform the reference skin mesh $\hat{M}_M$ to a new skin mesh $M_{M(\Phi)}$ in line with the articulation parameters ϕ of the skeleton, we employ Linear Blend Skinning (LBS) [19]. LBS updates vertices based on the skeleton's articulation via:

$$\boldsymbol{v_i} = \sum\nolimits_b w_{i,b} F_b \hat{\boldsymbol{v}}_i + \boldsymbol{t_b}, \tag{5}$$

with $\boldsymbol{t_b} = \boldsymbol{h_b} - F_b \hat{\boldsymbol{h}}_{\boldsymbol{b}}$ being a translation vector. The skinning weights $w_{i,b}$ capture how much vertex $\boldsymbol{v_i}$ is influenced by articulating bone b. They are obtained by solving a heat equilibrium analogy as described in [20].

During the pronation-supination movement of the lower arm, the amount of skin sliding gradually increases over the elongation axis of the arm. This twisting behavior cannot be explained with standard linear blend skinning since the expected skin deformation does not follow the transformation of its underlying bone. Instead, we model the skin deformation during pronation-supination by applying spherical linear interpolation (SLERP) [21] between C_{ulna} and C_{radius}, where the interpolation parameter t linearly increases from the ulna's head at the wrist to the radius' base at the elbow [9]. A vertex is then rotated with the interpolated rotation matrix depending on its location along the connection axis.

$$\boldsymbol{v_i} = \left[w_{i,ulna}\, t\, T_{ulna} + w_{i,radius}\, (1-t) T_{radius}\right] \hat{\boldsymbol{v}}_i. \tag{6}$$

2.2 Articulation-Based Registration

Hierarchical Optimization. The aim of this section is to fit the articulation model, described in the previous section, to a 3D surface scan, denoted by $M_T = (V_T, \varepsilon_T)$. This registration is done by optimizing a set of model parameters Ω via a non-linear Levenberg-Marquardt (LM) optimization scheme. The parameters include the articulation parameters, anthropometric scaling parameters, and rigid transformation parameters, summarized in Table 1. To avoid the optimizer ending in local minima, we subdivide the set Ω in several smaller groups of parameters $\Omega = \left\{\Phi_j = \{\phi_i\}_j\right\}$ and order the parameters in each group Φ_j in a hierarchical structure which is optimized iteratively (e.g. A, A-B, A-B-C) by the LM optimizer. By using a wrist-centered armature, we can decouple the hand and arm related parameters and do their registration steps independently. The order in which we optimize the defined parameter groups are: "hand", "arm", "rigid", "scaling", "rigid", "hand", and "arm". Furthermore, we optimize each finger independently.

Landmark-Based Initialization. Before starting the hierarchical iterative optimization protocol, we initialize the registration by globally scaling and aligning the reference hand based on three landmarks: two at opposite sides of the wrist and one at the middle fingertip. Additionally, the length of the arm is set based on the distance between landmarks at the wrist and an additional landmark at the elbow pit. This second step was performed due to missing elbow geometry in our scan dataset, and would not be required if the elbow is thoroughly scanned.

Table 1. Parameter hierarchy. The parameter set is divided in independent parameter groups Φ_j. Parameters in each group are organised in different levels, where each level is optimised at a time. Optimisation is done iteratively between levels within each group.

Group Φ_j	Level $\{\phi_i\}$	Degrees of freedom	Relevant bones $B \subset S$
Hand	A	α_{M3}, β_{M3}	M2–5, PP2–5
	B	α_{PP2-5}, β_{PP2-5}	PP2–5
	C	γ_{root}, α_{M3}, β_{M3}	M2–5, PP2–5
Arm	A	α_R, β_R	U, R
	B	δ_U	H
	C	α_H	H
Scaling	A	$s^{\perp}_{U,R,H}$, $s^{\perp}_{M1-5,PP1-5,PM2-5,PD1-5}$	U, R, M2–5, PP2–5
Rigid	A	Global translation and rotation	Root, M5
Thumb	A	α_{M1}, β_{M1}, α_{PP1}	PP1, PD1
	B	α_{PD1}	PP1, PD1
	C	α_{M1}, β_{M1}, α_{PP1}, α_{PD1}, $s^{//}_{M1,PP1,PD1}$, $s^{\perp}_{PP1,PD1}$	PP1, PD1
Finger *	A	α_{M*}, β_{M*}, α_{PP*}, β_{PP*}, α_{PM*}, α_{PD*}	PP*, PD*
	B	α_{PP*}, β_{PP*}, α_{PM*}, α_{PD*}, $s^{//}_{M*}$, $s^{//}_{PP*,PM*,PD*}$, $s^{\perp}_{PP*,PM*,PD*}$	PP*, PD*

Energy Function. At each hierarchy level, we apply a LM optimization to minimize

$$\phi = \arg\min_{\phi} \left(\sum_{i=1}^{|V_M|} w_a(i, B) \left| \min_j \left(d\left(V_{M(\phi)}(i), V_T^{//}(j) \right) \right) \right|^2 \right), \tag{7}$$

where w_a is a binary weight used to turn on and off the contribution of vertices, depending on whether its corresponding bone is in the set of bones B considered to be relevant for the optimisation (see Table 1). $V_T^{//}$ is the subset of V_T consisting of vertices whose normals are within 72° from the normal at $\boldsymbol{V_M}(\boldsymbol{i})$ (a more strict threshold of 37° is used for the scaling and arm optimisation steps). Rather than excluding points based on their normals, we search for the closest point that meets this normal angle condition. By doing so, we ensure that all points on the mesh will have a corresponding point (as long as the mesh is not too sparse). Points for which a counterpart was not found are excluded from the energy function.

The distance measure $d(\boldsymbol{p}, \boldsymbol{q})$ used is the point-to-plane distance introduced by Park and Subbarao [22]. This is beneficial over point-to-point distance when using low resolution mesh, but cannot be used for optimizing arm supination since corresponding reference and target vertices lie in the same plane. In that situation, we replace the distance measure by its point-to-point variant.

2.3 Shape Correspondences

Initially, the vertices in our 3D meshes are randomly ordered, meaning that, say, vertex $\boldsymbol{v_i}$ in our reference mesh does not anatomically correspond to vertex $\boldsymbol{v_i}$ in another hand mesh. The number of vertices may also be different for every mesh. Before performing statistical analysis on these meshes, we must first establish an anatomical correspondence between them. This correspondence is achieved in two steps. First, the articulation-based registration, described above, is performed to align our reference hand to the target mesh. Second, an elastic registration algorithm is applied to provide a more precise anatomical correspondence between the reference mesh and the target mesh [23]. The final result is that the reference surface is deformed to have its shape as similar as possible to the shape of the target surface. At this point, the target mesh is replaced by the deformed reference, ensuring that each hand mesh has the same number of vertices ordered in the same fashion. This consistent vertex order ensures that every hand mesh has the same vertices in the same anatomical positions.

2.4 Pose Normalization

In the statistical model, we are only interested in anthropometric variations and want to normalize as much as possible for any variation due to pose and articulation differences. Therefore, we apply a pose normalization on the elastically deformed mesh, using the skeleton estimated by articulation-based registration. Pose normalization can easily be achieved by interchanging the rest and pose articulations, i.e. inverting the

rest to pose transformation matrix in Eq. (2). Finally, all pose-normalized scans are centered around their center-of-gravity position.

2.5 Shape Modelling

To investigate the principal modes of variations present in the population, we apply a linear dimensionality reduction algorithm on the pose normalized registered scans. A popular choice for statistical shape modelling is a principal component analysis (PCA) [24]. In our context, PCA converts the vertex sets from all meshes into smaller sets of values through the definition of linearly uncorrelated variables called principal components. These principal components are defined by applying an orthogonal transformation on the original vertex coordinates. The position of vertex $\boldsymbol{v_i}$ in the statistical model is modelled as its average position $\boldsymbol{\mu_i}$ plus a linear combination of principal components $P_{i,j}$:

$$\boldsymbol{v_i} = \boldsymbol{\mu_i} + \sum\nolimits_j \boldsymbol{w_j} P_{i,j}. \tag{8}$$

The weights $\boldsymbol{w_j}$ give the contribution of each principal component (PC) to the model instance. The calculated PCs describe orthogonal directions of variance and they are ordered based on the fraction of variance found along the direction.

3 Results

In this section, we provide the results of the proposed registration and model-building techniques after testing them on a set of 100 static optical surface scans acquired with a 3dMD system. For comparison purposes, we also applied the elastic registration on the dataset as described in Sect. 2.3 but without the articulation-based initialization of Sect. 2.2.

3.1 Articulation-Based Registration

Anatomical Correspondence. To quantify the anatomical accuracy of the registration method, we annotated 22 anatomical landmarks on the reference mesh and on each target scan. Landmarks were annotated at anatomical feature locations: at the elbow pit, at two opposite points around the wrist, at each fingertip and at all finger joints. We calculated the distance between the landmark positions on the moving mesh and their ground-truth counterpart on the target mesh. These distances were computed after our articulation-based registration, after our elastic registration, and for the result of a purely elastic registration, without articulation-based initialization.

The landmark correspondence results are shown in Fig. 2(a). The average distance between joint landmarks after articulation and elastic registration was 5.7 mm, compared to 6.8 mm without the articulation based initialization step. Anatomical alignment is the best at the fingertips and distal joints because its estimation relies on clear geometric features. The accuracy on the elbow pit alignment is low due to missing data

at the elbow and limited geometry information at the upper arm. Given the improved landmark correspondence of our algorithm, we can conclude that the articulation-based registration - as an initialization step - improves the anatomical correspondence of the elastic registration.

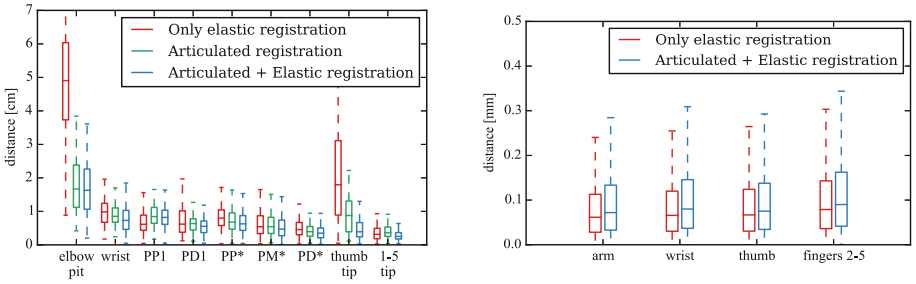

(a) Landmark correspondence error (b) Geometric error

Fig. 2. The anatomical and geometrical correspondence results for our registration method and a purely elastic method. Anatomical correspondence error, using expert-denoted landmarks, is shown in (a) while geometric errors in the hand shapes are shown in (b).

Geometric Correspondence. To create shape correspondence, we replace a target mesh by the registered result. This step may introduce geometric error where the surfaces do not match exactly. We quantify this geometric correspondence accuracy by calculating the average distance between the target and the elastically registered mesh, in the normal direction on the registered mesh. The results are shown in Fig. 2(b), with the average distance between surfaces grouped by anatomical region. The average geometric accuracy of our algorithm was 0.12 mm.

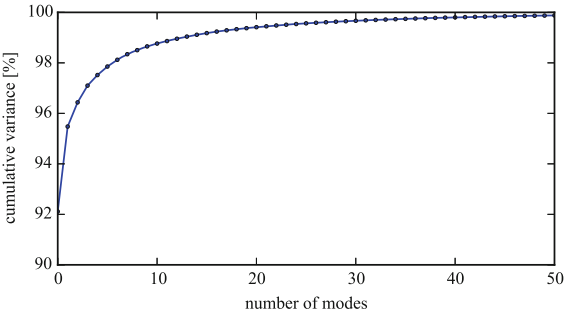

Fig. 3. Normalized compactness graph of the statistical hand shape model.

3.2 Statistical Model

Model Performance/Compactness. The compactness of a statistical model is a widely used measure to quantify how efficiently the model describes the total variance

in the population [25, 26]. The compactness measure $C(m)$ is defined as the sum of the shape variance captured by the first m principal components:

$$C(m) = \sum_{i=1}^{m} \lambda_i, \tag{9}$$

with λ_i the shape variance described by the ith PC. Figure 3 shows the normalized compactness results of our statistical hand shape model. The first principal component explains over 90% of the total variability in the dataset, while the first four PC account for over 97%.

Our model's first four principal components are visualized in Fig. 4. The average geometry is shown along with ± three standard deviations for each principal component. The first PC describes global scaling. The second PC describes variations in the length-to-thickness ratio of the arm, hand and fingers. The third and fourth PC are related to varying length and width of the fingers relative to arm size, respectively.

4 Discussion

We have presented a two-step registration method for 3D meshes of human hands. First, we matched an articulating prior model to a target scan, then we applied an elastic registration to obtain more precise shape correspondence. We demonstrated our method on a dataset of 100 optical 3D surface scans. We showed that the anatomical accuracy improves by 17% by initializing the elastic registration with the articulation-based registration result, while the average geometric accuracy stays around 0.12 mm. We further fed the registered surfaces into a statistical shape modelling algorithm and showed that the resulting model provides a compact representation of the population's variation. Only four principal components are needed to describe 97% of the shape variability in the dataset. We believe that our model is suitable for applications like hole-filling and resolution improvement, where pose estimation is an inevitable task. Our shape model could also be useful as a prior in a surface registration algorithm.

Nevertheless, our results did highlight a few limitations. We observed low accuracy on the estimation of the elbow pit location mainly due to missing data around the elbow and limited geometry at the upper arm. We also noted that the registration outcome highly depends on its settings (e.g. the ranges of motion, order of parameter optimizations, vertex normal thresholds). Finally, it is likely that some articulation information did make it into the shape model as a result of errors in the articulation-based registration. The source of these errors include the optimization settings, but also the limited degrees of freedom in the reference hand (e.g. the use of the golden ratio to scale finger bones). Our future work will look at addressing these limitations as well as extending the technique to the 4D modelling of hand motion.

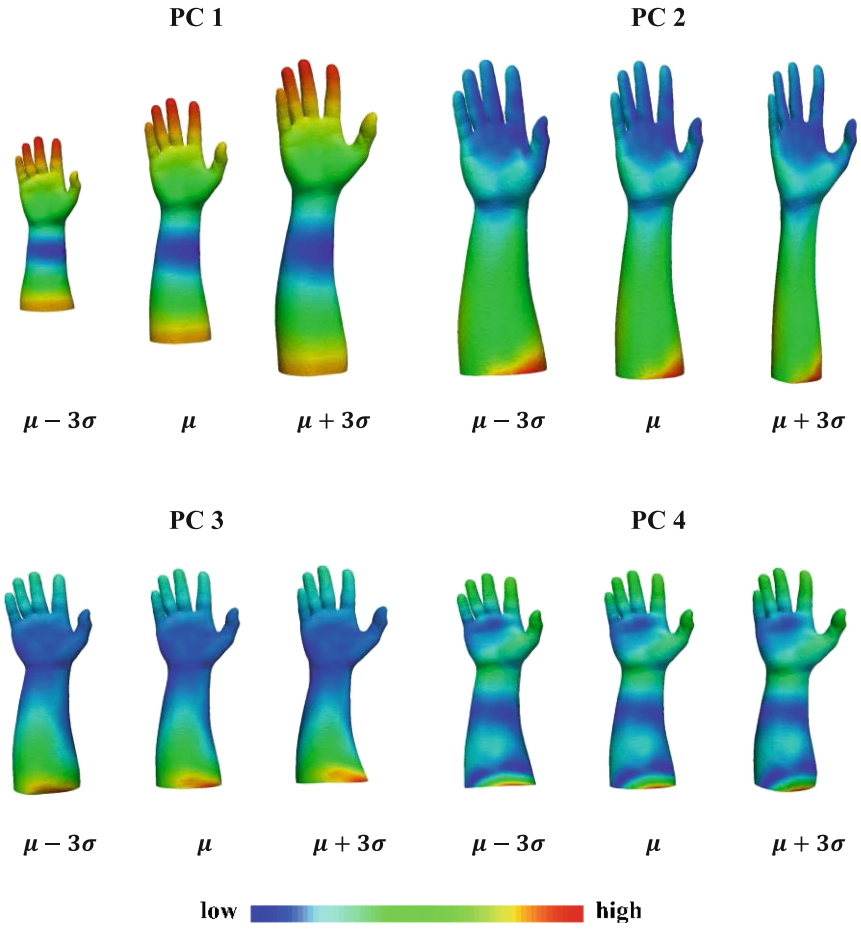

Fig. 4. First four eigenmodes of the statistical shape model. Color represents the variance $\lambda_i(j)$ for vertex j along the ith PC.

5 Conclusion

We presented herein a registration method for 3D meshes of human hands. It was based on the alignment of an articulating reference hand and elastic deformation. We demonstrated the registration's effectiveness by building a PCA shape model of the human hand. In the future, we will improve the anatomical accuracy of the methodology and to extend the method to model hand motion.

Acknowledgments. This work was supported by the Research Foundation in Flanders (FWO SB) and the VLAIO PLATO-project. The authors would like to thank Vigo nv, More Institute vzw and Orfit Industries nv for their continued contribution to the project.

References

1. Blanz, V., Vetter, T.: A morphable model for the synthesis of 3D faces. In: 26th Annual Conference on Computer Graphics and Interactive Techniques, pp. 187–194 (1999)
2. Hasler, N., et al.: A statistical model of human pose and body shape. Comput. Graph. Forum **28**(2), 337–346 (2009)
3. Anguelov, D., et al.: SCAPE: shape completion and animation of people. ACM Trans. Graph. **24**(3), 408–416 (2005)
4. Harih, G., Tada, M.: Development of a finite element digital human hand model. In: 7th International Conference on 3D Body Scanning Technologies, pp. 208–213 (2016)
5. Tagliasacchi, A., et al.: Robust articulated-ICP for real-time hand tracking. Comput. Graph. Forum **34**(5), 101–114 (2015)
6. Taylor, J., et al.: User-specific hand modeling from monocular depth sequences. In: IEEE Conference on Computer Vision and Pattern Recognition, pp. 644–651 (2014)
7. Oikonomidis, I., et al.: Evolutionary quasi-random search for hand articulations tracking. In: IEEE Conference on Computer Vision and Pattern Recognition, pp. 3422–3429 (2014)
8. Sharp, T., et al.: Accurate, robust, and flexible real-time hand tracking. In: 33rd Annual ACM Conference on Human Factors in Computing Systems, pp. 3633–3642 (2015)
9. Zhu, L., et al.: Adaptable anatomical models for realistic bone motion reconstruction. Comput. Graph. Forum **34**(2), 459–471 (2015)
10. Tan, D.J., et al.: Fits like a glove: rapid and reliable hand shape personalization. In: IEEE Conference on Computer Vision and Pattern Recognition, pp. 5610–5619 (2016)
11. Khamis, S., et al.: Learning an efficient model of hand shape variation from depth images. In: IEEE Conference on Computer Vision and Pattern Recognition, pp. 2540–2548 (2015)
12. Lübbers, H.-T., et al.: Precision and accuracy of the 3dMD photogrammetric system in craniomaxillofacial application. J. Craniofac. Surg. **21**(3), 763–767 (2010)
13. Grothausmann, R.: Providing values of adjacent voxel with vtkDiscreteMarchingCubes (2016)
14. Visual Computing Lab ISTI CNR: MeshLab. http://www.meshlab.sourceforge.net
15. Valette, S., Chassery, J.-M.: Approximated centroidal voronoi diagrams for uniform polygonal mesh coarsening. Comput. Graph. Forum **23**(3), 381–389 (2004)
16. Wu, G., et al.: ISB recommendation on definitions of joint coordinate systems of various joints for the reporting of human joint motion—Part II: shoulder, elbow, wrist and hand. J. Biomech. **38**(5), 981–992 (2005)
17. James, F.: Minuit-a system for function minimization and analysis of the parameter errors and correlations. Comput. Phys. Commun. **10**(6), 343–367 (1975)
18. Park, A.E., et al.: The Fibonacci sequence: relationship to the human hand. J. Hand Surg. Am. **28**(1), 157–160 (2003)
19. Lewis, J.P., et al.: Pose space deformation. In: 27th Annual Conference on Computer Graphics and Interactive Techniques, pp. 165–172 (2000)
20. Baran, I., Popovi, J.: Automatic rigging and animation of 3D characters. ACM Trans. Graph. Artic. **26**(3), 72 (2007)
21. Shoemake, K., et al.: Animating rotation with quaternion curves. In: ACM SIGGRAPH Computer Graphics, pp. 245–254 (1985)
22. Park, S.-Y., Subbarao, M.: An accurate and fast point-to-plane registration technique. Pattern Recognit. Lett. **24**(16), 2967–2976 (2003)
23. Danckaers, F., et al.: Correspondence preserving elastic surface registration with shape model prior. In: 22nd International Conference on Pattern Recognition, pp. 2143–2148 (2014)

24. Cootes, T.F., et al.: Active shape models-their training and application. Comput. Vis. Image Underst. **61**(1), 38–59 (1995)
25. Davies, R.H., et al.: A minimum description length approach to statistical shape modelling. IEEE Trans. Med. Imaging **21**(5), 525–537 (2002)
26. Su, Z.: Statistical Shape Modelling: Automatic Shape Model Building. University College London (2011)